

Modeling of Mixed-Mode Fracture of Rock under Different Environments by Configurational Mechanics

Chao Wang^{a,b}, Hongze Li^{a,b}, J.L. Feng^{a,b,2}, Jiaqi Zhang^{a,b} and D.J. Li^{a,b}

^aState Key Laboratory for Tunnel Engineering, China University of Mining and Technology Beijing, D11 Xueyuan Rd, Haidian District, 100083, Beijing, China

^bSchool of Mechanics and Civil Engineering, China University of Mining and Technology Beijing, D11 Xueyuan Rd, Haidian District, 100083, Beijing, China

ARTICLE INFO

Keywords:

Configurational mechanics, Rock fracture criterion, Plastic zone, Mohr-Coulomb yield criterion, Environmental effects


ABSTRACT


We study mixed-mode fracture problems of rock under thermal conditions, using configurational mechanics. The interpretation of configurational stress tensor is realized by the principle of energy conservation. The Mohr-Coulomb yield criterion in term of configurational stress is used to determine the boundary of crack-tip plastic zone. A fracture criterion is proposed by the local properties of the crack-tip plastic zone while the time factor in Burgers body is introduced to address the rheological fracture properties of rock. By the present fracture criterion, the impacts of the drying-wetting cycle, heating-cooling cycle, thermal treatment and chemical corrosion on rock fracture are examined. The results show that the components of configurational stress tensor represent the change of total energy induced by material element translation. It is concluded that the crack-tip plastic zone assessed by the present yield criterion is more reasonable in the size and shape while the initiation angle and fracture load predicted by the present fracture criterion are consistent with those predicted by the maximum tensile stress criterion. It is also found that the fracture loads of rock decrease with the drying-wetting cycles and heating-cooling cycles. Furthermore, the analysis indicates that the crack-tip plastic zone in rock enlarges with time elapse while the fracture load envelope decreases. Finally, the fracture load envelope of rock decreases with the thermal treatment temperature increase generally, and the fracture resistance is the minimum in acidic environments.

Understanding the way rocks break is a question relevant to many diverse areas such as earthquake mechanics, earthquake prediction, hydraulic fracturing, landslides, mining sciences, tunneling mechanics, and civil engineering [6, 13, 15, 36, 37, 41, 42, 51]. At a fundamental level, the determination of the precise mechanism at the initiation of rock fracture under complex stress conditions is one of the most active fields of research. On the one hand, the stability and safety of rock structure may be impacted by the fracture mechanical properties, which are determined by the structure and composition. On the other hand, such rock structure and its ingredients are also affected by high temperature, chemical corrosion, and high stress conditions, which deteriorate the mechanical properties. Most importantly, rock failure initially occurs under complicated mixed-mode conditions and complex environments. Another issue is that a crack frequently initiates and propagates in rock after a period of time when the initial stress intensity factor is less than the fracture toughness. This implicitly indicates that rock fracture is accompanied by a process of time-dependent subcritical cracking, in which rock exhibits its rheological fracture behaviors that are with the characters of decay and steady creep stages [55, 48]. In the past decades, fracture criteria such as the maximum energy release rate criterion (MERR) [22], the maximum tensile stress criterion (MTS) [9], and the minimum strain energy density criterion [4] have been proposed to evaluate the fracture behaviors of material under complex mode crack. To rocks, the corresponding fracture mechanisms are more intricate and difficult to understand.

Generally speaking, there is almost always a plastic zone at the crack tip surrounded by an elastic zone to most brittle materials. The properties of crack-tip plastic zone are vital for fatigue and fracture assessments of defects. Therefore, some fracture criteria based on yield functions are proposed, including Mohr-Coulomb fracture criterion [5] and R criterion [45, 23]. Mixed-mode fracture is a result of the variability of mechanical characteristics in rocks and the complexity of external loads. Much work of rock fracture tests is to clarify the fracture behaviors such as crack initiation and propagation mechanism in rocks. Lim et al. [28, 29] conducted mode I and mixed mode I-II fracture tests of soft

*Corresponding author

 fjl@cumtb.edu.cn (J.L. Feng)

 www.cumtb.edu.cn (J.L. Feng)

ORCID(s): 0000-0003-4689-2596 (J.L. Feng)

rocks under three-point bending conditions. Aliha et al. [1] presented the mixed fracture resistance envelope of marble from fracture tests using cracked semi circular bend (SCB) specimens, and verified by the generalized MTS fracture criterion considering T stress. Yang and Jing [53] examined the fracture process of sandstone with a single fissure under uniaxial compression, and found that there exist nine different crack types based on their geometry and crack propagation mechanisms. To evaluate factors that reduce rock fracture toughness, Han et al. [20] conducted fracture tests of sandstone specimens immersed in various chemical solutions, and found that the fracture toughness decreases with corrosion time. Gan et al. [12] conducted rock fracture tests employing centrally cracked Brazilian disc specimens after thermal-chemical treatment and found that the temperature and chemical solution can mutually complement and promote each other. To further understand the thermal effects of rock fracture, Zuo et al. [56] investigated the influence of temperature on the fracture behavior of siltstone by using three-point bending fracture tests and found that the fracture toughness firstly decreases, then increases, and eventually declines with temperature increase. Peng et al. [39] summarized that the fracture toughness and equivalent fracture toughness all gradually reduced with the temperature increase conducting semi-circular three-point bending tests. Guo et al. [16] found that the fracture toughness and elasticity modulus of marble decreases as the temperature increases from 20 to 800 °C in three-point bending tests.

In linear elastic fracture mechanics (LEFM), the energy release rate serves as the crack driving force. If it exceeds the crack propagation resistance, the crack starts to propagate. Configurational mechanics is generally used to address problems of defect movement [19, 18, 32, 33]. The configurational force and configurational stress constitute the configurational force balance equation in the material configuration, governing material motion. Configurational stress, also known as energy momentum tensor or Eshelby stress, was originally proposed by Eshelby to evaluate the forces acting on defects [10, 11]. Furthermore, the configurational force or stress can be employed to evaluate conservation integrals in fracture mechanics [3], such as J_k ($k = 1, 2$), M , and L , representing the translation, rotation, and self-similar expansion of cracks, respectively. Simha et al. [43] calculated the J integral and crack driving force in elastic-plastic materials using configurational force method, and found that J integral is path dependent in incrementally plastic materials. Gross et al. [14] provided specific applications of the configurational force approach for various defects in points, lines, surfaces and volumes. Muller et al. [35] presented the discrete node configurational force using finite element method, and found that the configurational force approach can check and improve the finite element solution. Menzel and Steinmann [34, 44] derived the balance equations in different configurations for elastic-plastic materials based on the multiplicative decomposition of the deformation gradient tensor, providing the volume forces and PeachKoehler force. The configurational force is also suitable to represent the material damage. Liebe et al. [27] and Dascalu et al. [8] applied the configurational force approach to damage materials, providing the discrete node point forces for different damage states combined with finite element method. Additionally, the configurational force/stress can also be used to develop fracture criteria. For example, Kienzler and Herrmann [24, 26] established a fracture criterion based on the local properties of configurational stress tensor. Based on their work, Guo et al. [17], Liu et al. [30] and Lv et al. [31] developed fracture criteria based on the configurational force vector and equivalent configurational stress, and their predicted results coincided well with experiments and other theoretical results. We [47] recently proposed some configurational stress-based fracture criteria based on the critical area of crack-tip plastic zone to examine the crack initiation mechanism of material. These studies demonstrated that the configurational force method is an effective tool for solving material motion problems such as material structure evolution or defect motion.

Even though many rock fracture tests have been conducted under different conditions as the previously mentioned, there is still a lack of well-established theoretical models to properly explain these experimental results. With regard to rock fracture model we primarily attempted to study it by the configurational force method [46], however it still needs to be explored, specifically including the rheological fracture effects of viscoelastic rock and the crack initiation mechanism under complex stresses and chemical environments. This work is to develop a fracture criterion of rock based on the configurational mechanics together with the Mohr-Coulomb yield criterion to understand the mixed-mode fracture mechanisms of rock under complex environmental conditions. By the analysis of crack-tip plastic zone characteristics, we take the critical area of crack-tip plastic zone as a key parameter to assess fracture load. Additionally, the impact of irregular cracks, drying-wetting and heating-cooling cycles on rock fracture are investigated as well. Furthermore, time factors are introduced to study the viscoelastic fracture behaviors of rocks. Finally, the thermal treatment temperature and pH are considered to evaluate the fracture loads of rocks at different temperatures and chemical environments (pHs).

1. Governing equations by configurational mechanics

In contrast to Cauchy stress in the current configuration, configurational stress is represented in the material configuration. As a result, it has an advantage in dealing with material motion problems. We here conceptually derive the configurational stress tensor and provide a physical interpretation within the context of thermodynamics.

It is noted that the Lagrangian density L can be defined as within the framework of dynamics,

$$L = K - W = \frac{1}{2}\rho_0(\mathbf{x})\mathbf{v}^2 - W(\mathbf{x}, \boldsymbol{\varepsilon}) \quad (1)$$

where K denotes the kinetic energy, W the potential energy, ρ_0 the density of the body, \mathbf{v} the velocity of material point, and $\boldsymbol{\varepsilon}$ the strain tensor.

By the principle of energy conservation, the linear-momentum equations in the current configuration are given by

$$\text{Div} \boldsymbol{\sigma} + \mathbf{f} = \rho_0 \dot{\mathbf{v}}, \quad \boldsymbol{\sigma} = \frac{\partial W}{\partial \boldsymbol{\varepsilon}}, \quad \boldsymbol{\varepsilon} = \frac{1}{2} (\nabla \mathbf{u} + (\nabla \mathbf{u})^\top) \quad (2)$$

where $\boldsymbol{\sigma}$ denotes the Cauchy stress, and \mathbf{f} the body force per unit volume in the current configuration.

Evaluating the gradient of L , one has

$$\nabla_k L = L_{,k} = \frac{1}{2} \nabla_k \rho_0 v_i v_i + \rho_0 v_i v_{i,k} - \left. \frac{\partial W}{\partial x_k} \right|_{\text{expl.}} - \frac{\partial W}{\partial \varepsilon_{ij}} \varepsilon_{ij,k} \quad (3)$$

where $|_{\text{expl.}}$ denotes the explicit dependence of W on x_k .

By the divergence theorem, it follows that

$$\sigma_{ij} \varepsilon_{ij,k} = (\sigma_{ij} u_{i,k})_{,j} - u_{i,k} \sigma_{ij,j} = (\sigma_{ij} u_{i,k})_{,j} - (\rho_0 \dot{v}_i - f_i) u_{i,k}, \quad L_{,k} = \text{Div}(L \delta_{jk}) \quad (4)$$

The linear momentum equation in the material configuration is derived by

$$\text{Div}_j (-L \delta_{jk} - \sigma_{ij} u_{i,k}) - \left. \frac{\partial W}{\partial x_k} \right|_{\text{expl.}} + \frac{1}{2} \nabla_k \rho_0 v_i v_i + \rho_0 \frac{\partial}{\partial t} (v_i u_{i,k}) - u_{i,k} f_i = 0 \quad (5)$$

From Eq (5), $\boldsymbol{\Sigma}^K$ and \mathbf{g}^K are defined by

$$\boldsymbol{\Sigma}^K = (W - K) \mathbf{I} - \nabla^\top \mathbf{u} \boldsymbol{\sigma}, \quad \mathbf{g}^K = - \left. \frac{\partial W}{\partial \mathbf{x}} \right|_{\text{expl.}} + \frac{1}{2} \nabla \rho_0 \mathbf{v}^2 - (\nabla \mathbf{u})^\top \mathbf{f} \quad (6)$$

where \mathbf{I} is the 2nd order identity tensor. For the static or quasi-static problems, the traditional configurational force balance equation is simplified as follows,

$$\text{Div} \boldsymbol{\Sigma} + \mathbf{g} = \mathbf{0} \quad (7)$$

and Eq (6) is reduced to as

$$\boldsymbol{\Sigma} = W \mathbf{I} - (\nabla \mathbf{u})^\top \boldsymbol{\sigma}, \quad \mathbf{g} = - \left. \frac{\partial W}{\partial \mathbf{x}} \right|_{\text{expl.}} + (\nabla \mathbf{u})^\top \mathbf{f} \quad (8)$$

It is noted that Eq (8) is the Eshelby stress or energy momentum tensor originated by Eshelby, which can be used to explore the material structural evolution and defects movement. If considering finite deformation issue, Eq (8) is rewritten as follows,

$$\boldsymbol{\Sigma} = W \mathbf{I} - \mathbf{F}^\top \mathbf{P}, \quad \mathbf{g} = - \left. \frac{\partial W}{\partial \mathbf{x}} \right|_{\text{expl.}} + \mathbf{F}^\top \mathbf{b} \quad (9)$$

where \mathbf{P} represents the first Piola-Kirchhoff tensor, \mathbf{F} indicates the deformation gradient, and \mathbf{b} is the body force per unit volume in the reference configuration.

In linear elastic fracture mechanics, configurational stress/force can be used to calculate the J integral, as shown in Figure 1(b). Let us consider a circle Γ_r with a radius r , so that we have

$$J_{\text{far}} - J_{\text{tip}} = \mathbf{e} \cdot \int_{\Gamma_r} \boldsymbol{\Sigma} \cdot \mathbf{n} ds - J_{\text{tip}} = \int_{\Omega} g da \quad (10)$$

where \mathbf{e} is the crack tip propagation direction that is determined by $\mathbf{v}_{\text{tip}}/|\mathbf{v}_{\text{tip}}|$. Equation (10) indicates the path-independence of J integral if $g = 0$.

Configurational force, as the driving force of defect, can be calculated by the negative gradient of the total energy. Naturally, the configurational stress can also be explained by the principle of energy conservation in the process of the translation of infinitesimal element.

If a body B is with volume Ω , then the total energy of the body is

$$\begin{cases} \Pi^{\text{tot}} = \Pi^e + \Pi^i \\ \Pi^i = \int_{\Omega} W(x_k) dv \end{cases} \quad (11)$$

where Π^e denotes the work done by the surface traction, Π^i the total internal energy.

If the element moves along the x -axis at λ_1 as shown in Figs 1 and 2 as well as considering the face @, then it is calculated by

$$\begin{cases} \Delta \Pi_a^i = -W \lambda_1 dx_2 \\ \Delta \Pi_a^e = \sigma_{11} u_{1,1} \lambda_1 dx_2 + \sigma_{12} u_{2,1} \lambda_1 dx_2 \\ \Delta \Pi_a^{\text{tot}} = - (W - \sigma_{11} u_{1,1} - \sigma_{12} u_{2,1}) \lambda_1 dx_2 \end{cases} \quad (12)$$

Similarly, for the face b, $\Delta \Pi^i$ and $\Delta \Pi^e$ are computed by

$$\begin{cases} \Delta \Pi_b^i = \delta \Pi_d^i = 0 \\ \Delta \Pi_b^e = - (-\sigma_{21} u_{1,1} - \sigma_{22} u_{2,1}) \lambda_1 dx_1 \end{cases} \quad (13)$$

On the other hand, if the element moves along the y -axis at λ_2 , the change of total energy is calculated by

$$\begin{cases} \Delta \Pi_b^i = -W \lambda_2 dx_1 \\ \Delta \Pi_b^e = (\sigma_{21} u_{1,2} + \sigma_{22} u_{2,2}) \lambda_2 dx_1 \\ \Delta \Pi_b^{\text{tot}} = - (W - \sigma_{21} u_{1,2} - \sigma_{22} u_{2,2}) \lambda_2 dx_1 \end{cases} \quad (14)$$

and

$$\begin{cases} \Delta \Pi_a^i = \Delta \Pi_c^i = 0 \\ \Delta \Pi_a^e = (\sigma_{11} u_{1,2} + \sigma_{12} u_{2,2}) \lambda_2 dx_2 \\ \Delta \Pi_a^{\text{tot}} = - (\sigma_{11} u_{1,2} - \sigma_{12} u_{2,2}) \lambda_2 dx_2 \end{cases} \quad (15)$$

From the above derivation, it is observed that the component of configurational stress tensor Σ_{ij} represents the change of total energy with respect to an infinitesimal element translation in the x_j direction of an oriented unit element of area projected in the x_i direction.

If the strain energy density in elastic body $W = 1/2 \sigma_{ij} u_{i,j}$, combined with $\Sigma_{ij} = W \delta_{ij} - \sigma_{ij} u_{i,j}$, then we have

$$\begin{cases} \Sigma_{11} = -\frac{1}{2} \sigma_{11} u_{1,1} - \frac{1}{2} \sigma_{12} u_{2,1} + \frac{1}{2} \sigma_{21} u_{1,2} + \frac{1}{2} \sigma_{22} u_{2,2} \\ \Sigma_{12} = -\sigma_{11} u_{1,2} - \sigma_{12} u_{2,2} \\ \Sigma_{21} = -\sigma_{21} u_{1,1} - \sigma_{22} u_{2,1} \\ \Sigma_{22} = \frac{1}{2} \sigma_{11} u_{1,1} + \frac{1}{2} \sigma_{12} u_{2,1} - \frac{1}{2} \sigma_{21} u_{1,2} - \frac{1}{2} \sigma_{22} u_{2,2} \end{cases} \quad (16)$$

The underlying configurational force can be evaluated by the projection of the configurational stress tensor, as shown in Figure 3(b). J -integral is calculated by

$$J = \int_{-\pi}^{\pi} (\Sigma_{11}n_1 + \Sigma_{21}n_2) ds = (K_I^2 + K_{II}^2)/E \quad (17)$$

where K_I and K_{II} are the stress intensity factors of mode-I and mode-II cracks, respectively.

The configurational stress tensor is asymmetric so that its trace is zero, as shown in Fig 3(a). Such asymmetric stress can be used to construct a symmetric one by multiplying the third order Levi-Civita tensor,

$$\Sigma_{ij}^M = \epsilon_{3ki} \Sigma_{jk} = \begin{bmatrix} -\Sigma_{12} & \Sigma_{11} \\ -\Sigma_{22} & \Sigma_{21} \end{bmatrix} \quad (18)$$

For the sake of convenience, it is assumed $\Sigma_{ij} = \Sigma_{ij}^M$, so that the configurational stress now is symmetric, which can be employed to replace Cauchy stress for predicting damage and fracture.

The configurational force balance equation can be discretized using the finite element method to calculate nodal configurational forces [35, 40]. Uniaxial tensile plane strain elastic bodies with mode I and mixed I-II cracks, respectively, are established by finite element method. The models are with width and height 50×100 mm, elastic modulus 20 GPa, Poisson's ratio 0.25. As shown in Fig 4, configurational forces for mode I cracks are found to be the greatest, followed by I-II mixed mode cracks. It is also indicated that the configurational forces are more sensitive to cracks, which mean that such underlying forces justify to characterize the mechanical behavior of cracks.

2. Crack-tip plastic zone by Mohr-Coulomb yield criterion

The Mohr Coulomb yield criterion is widely utilized to describe the failure of geo-materials due to its only two parameters, i.e., cohesive force and friction angle, which are easy to be determined in the laboratory, as shown in Fig 5. Indeed, accurate prediction of the crack-tip plastic zone is critical to evaluate the fracture mechanism and mechanical properties of rocks. As a consequence, it is justified to use the Mohr-Coulomb yield criterion to determine the plastic zone at the crack tip. It is assumed herein that the following entire derivations are accomplished in the K field and under the small scale yield (SSY) conditions. It is also noted that this section is an important part of the present fracture criteria.

For an isotropic cracked body under mixed mode I-II conditions, the singular stress components at the crack tip are given by [2],

$$\begin{cases} \sigma_{11} = \frac{K_I}{\sqrt{2\pi r}} \cos \frac{\theta}{2} \left(1 - \sin \frac{\theta}{2} \sin \frac{3\theta}{2} \right) - \frac{K_{II}}{\sqrt{2\pi r}} \sin \frac{\theta}{2} \left(2 + \cos \frac{\theta}{2} \cos \frac{3\theta}{2} \right) \\ \sigma_{22} = \frac{K_I}{\sqrt{2\pi r}} \cos \frac{\theta}{2} \left(1 + \sin \frac{\theta}{2} \sin \frac{3\theta}{2} \right) + \frac{K_{II}}{\sqrt{2\pi r}} \sin \frac{\theta}{2} \cos \frac{\theta}{2} \cos \frac{3\theta}{2} \\ \sigma_{12} = \frac{K_I}{\sqrt{2\pi r}} \cos \frac{\theta}{2} \sin \frac{\theta}{2} \cos \frac{3\theta}{2} + \frac{K_{II}}{\sqrt{2\pi r}} \cos \frac{\theta}{2} \left(1 - \sin \frac{\theta}{2} \sin \frac{3\theta}{2} \right) \end{cases} \quad (19)$$

where (r, θ) are the polar coordinates centered at the crack tip, K_I and K_{II} are the stress intensity factors (SIFs). Referring the angled crack problem, SIFs are read by

$$\begin{cases} K_I = K \cos \beta, & K_{II} = K \sin \beta \\ K = \sqrt{K_I^2 + K_{II}^2} \end{cases} \quad (20)$$

where K represents the effective stress intensity factor.

Substituting Eq (19) into Eq (16), then one has

$$\Sigma_{11} = \frac{(1+\kappa)}{64G\pi r} [2(K_I - K_{II})(K_I + K_{II}) \sin 3\theta + 12K_I K_{II} \cos \theta + 4K_I K_{II} \cos 3\theta + 2(K_I^2 - 5K_{II}^2) \sin \theta] \quad (21)$$

$$\Sigma_{22} = \frac{(1+\kappa)}{8G\pi r} \sin \theta (K_{II} \cos \theta + K_I \sin \theta)^2 \quad (22)$$

$$\Sigma_{12} = \frac{(1 + \kappa)}{8G\pi r} \cos \theta (K_{II} \cos \theta + K_I \sin \theta)^2 \quad (23)$$

where, $\kappa = \frac{3-\nu}{1+\nu}$ for plane stress, and $\kappa = 3 - 4\nu$ for plane strain, and $G = \frac{E}{2(1+\nu)}$.

Additionally, the principal stress at the crack-tip for mode-I fracture with $\theta = [0, \pi]$ is calculated by

$$\begin{aligned} \sigma_1 &= \frac{K_I}{\sqrt{2\pi r}} \cos \frac{\theta}{2} \left(1 + \sin \frac{\theta}{2} \right) \\ \sigma_2 &= \frac{K_I}{\sqrt{2\pi r}} \cos \frac{\theta}{2} \left(1 - \sin \frac{\theta}{2} \right) \\ \sigma_3 &= \begin{cases} \frac{2\nu K_I}{\sqrt{2\pi r}} \cos \frac{\theta}{2} & \text{for plane strain} \\ 0 & \text{for plane stress} \end{cases} \end{aligned} \quad (24)$$

In Cauchy principal stress space, the Mohr-Coulomb yield criterion is expressed mathematically by [7]

$$\begin{cases} \tau_n = c - \sigma_n \tan \varphi \\ f(\sigma_1, \sigma_2, \sigma_3) = \frac{1}{2}(\sigma_1 - \sigma_3) + \frac{1}{2}(\sigma_1 + \sigma_3) \sin \varphi - c \cos \varphi = 0 \end{cases} \quad (25)$$

where c and φ denote the cohesion and friction angle, and σ_n is the normal stress, positive in tension assumed here, as shown in Fig 5(a).

For plane stress problems, substituting Eq (24) into Eq (25), then the crack-tip plastic zone polar radius is obtained

$$r_p = \left[\frac{(1 + \sin \varphi) K_I \cos \frac{\theta}{2}}{2\sqrt{2\pi c} \cos \varphi} \left(1 + \sin \frac{\theta}{2} \right) \right]^2 \quad (26)$$

For plane strain problems, the plastic zone radius is written by a piecewise function

$$r_p = \begin{cases} \left[\frac{K_I \cos \frac{\theta}{2}}{2\sqrt{2\pi c} \cos \varphi} \left(1 - 2\nu + \sin \varphi + 2\nu \sin \varphi + (1 + \sin \varphi) \sin \frac{\theta}{2} \right) \right]^2, & 0 \leq \theta \leq 2 \sin^{-1}(1 - 2\nu) \\ \left[\frac{K_I \cos \frac{\theta}{2}}{\sqrt{2\pi c} \cos \varphi} \left(\sin \varphi + \sin \frac{\theta}{2} \right) \right]^2, & 2 \sin^{-1}(1 - 2\nu) \leq \theta \leq \pi \end{cases} \quad (27)$$

Figure 6 shows the crack-tip plastic zone assessed by the Mohr-Coulomb yield criterion, and the unit is $K_I^2/(\pi c^2)$ for mode-I cracks and $K_{II}^2/(\pi c^2)$ for mode-II cracks. It is observed that the plastic zone enlarges with the friction angles.

On the other hand, since the Mises yield function is frequently used to predict material plastic behavior,

$$(\sigma_{11} - \sigma_{22})^2 + (\sigma_{11} - \sigma_{33})^2 + (\sigma_{22} - \sigma_{33})^2 + 6(\sigma_{12}^2 + \sigma_{13}^2 + \sigma_{23}^2) = 2\sigma_s^2 \quad (28)$$

we here use it to assess the crack-tip plastic zone, as shown in Fig 7(a) where the unit is $K^2/(\pi \sigma_s^2)$.

Furthermore, the Mises configurational stress is also employed to calculate the crack-tip plastic zone, as shown in Fig 7(b), where the unit is $(1 + \kappa)/(G\pi \sigma_s^2) K^2$. It is observed that the size and shape in the plastic zone assessed by the Mises Cauchy stress are consistent with that predicted by the Mises configurational stress. The Mises configurational stress is read as [25]

$$(\Sigma_{11} - \Sigma_{22})^2 + (\Sigma_{11} - \Sigma_{33})^2 + (\Sigma_{22} - \Sigma_{33})^2 + 6(\Sigma_{12}^2 + \Sigma_{13}^2 + \Sigma_{23}^2) = 2\Sigma_s^2 \quad (29)$$

Evidently, the Mises yield function of configurational stress has better predictive effects on the plastic zone at the crack tip, whereas for rock materials, it is essential to investigate the local properties of the Mohr-Coulomb yield criterion based on configurational stress. In the present work, the Mohr-Coulomb yield criterion based on configurational stress is expressed as follows

$$f(\Sigma_1, \Sigma_2) = \frac{1}{2}(\Sigma_1 - \Sigma_2) + \frac{1}{2}(\Sigma_1 + \Sigma_2) \sin \varphi - c_\Sigma \cos \varphi = 0 \quad (30)$$

where c_Σ is determined by c^2/E , and Σ_1 and Σ_2 are derived by combining with Eqs (21), (23) and (22),

$$\begin{cases} \Sigma_{1,2} = \frac{1+\kappa}{32G\pi r} \left[4K_I K_{II} \cos \theta + 2(K_I - K_{II})(K_I + K_{II}) \sin \theta \pm \sqrt{2f(K_I, K_{II}, \theta)} \right] \\ f(K_I, K_{II}, \theta) = (K_I^2 + K_{II}^2) (K_I^2 + 5K_{II}^2 - (K_I^2 - 3K_{II}^2) \cos 2\theta + 4K_I K_{II} \sin 2\theta) \end{cases} \quad (31)$$

Eventually, the polar radius of the plastic zone is deduced

$$r_p = \frac{1+\kappa}{32G\pi c_\Sigma \cos \varphi} \left[2 \sin \varphi (2K_I K_{II} \cos \theta + (K_I^2 - K_{II}^2) \sin \theta) + \sqrt{2f(K_I, K_{II}, \theta)} \right] \quad (32)$$

The plastic zones in terms of Eq (30) are plotted on the left side of Fig 8, and the unit is $\frac{1+\kappa}{G\pi c^2} K^2$. It is found that the mode-I crack-tip plastic zone is asymmetric about the crack surface.

To obtain better results, a novel Mohr-Coulomb yield criterion based on configurational stress is proposed by

$$f(\Sigma_1, \Sigma_2) = \frac{1}{2}(\Sigma_1 - \Sigma_2) + \frac{1}{2}|\Sigma_1 + \Sigma_2| \sin \varphi - c_\Sigma \cos \varphi = 0 \quad (33)$$

The predicted results in terms of Eq (33) are given on the right side of Fig 8, where the unit is $\frac{1+\kappa}{G\pi c^2} K^2$. It is observed that the crack-tip plastic zone is continuous at the crack surface and its size, shape and relative placements of corner points agree with those in Figs 6 and 7. It is also found that the boundary of the crack-tip plastic zone enlarges with internal friction angles.

In summary, the crack-tip plastic zone is assessed using the Mohr-Coulomb yield criterion, Eq (33), which is with the character of symmetry. The present two Mohr-Coulomb yield criteria base on the configurational stress methods can be used to evaluate the crack-tip plastic zone of rock. More crucially, this plastic zone that is used to develop fracture criteria is discussed in the next section.

3. Mixed-mode fracture mechanism of rock

3.1. Fracture criteria established by the crack-tip plastic zone

Plastic deformation at the crack tip is related to material fracture. Fracture energy, according to the Griffith energy criterion, includes surface energy and plastic work. Thus the mechanical behavior of cracks can be predicted by the crack-tip plastic zone. It is noted that the R criterion [23] states that the crack initiates if the minimum radius for the crack-tip plastic zone reaches the critical value along the direction in which the radius possesses the minimum, as mathematically expressed by

$$\begin{cases} \frac{dr_p}{d\theta} = 0, & \frac{d^2 r_p}{d\theta^2} > 0 \\ r = r_C \end{cases} \quad (34)$$

Undoubtedly, the area of crack-tip plastic zone is better than its radius to represent the energy dissipation around the crack-tip. As a consequence, the crack initiates if the area of the plastic zone reaches or exceeds the critical value, as shown in Fig 9. Thus the present fracture criterion is formulated by

$$\begin{cases} \frac{dr_p}{d\theta} = 0, & \frac{d^2 r_p}{d\theta^2} > 0 \\ A_P = A_C \end{cases} \quad (35)$$

Combining Eq (33) with (35), a fracture criterion based on the plastic zone assessed by the MC yield criterion based on configurational stress is naturally presented, namely MCCS fracture criterion.

Apparently, it is difficult to obtain an analytical solution for the plastic zone area assessed by Eq (33) so that the Simpson's integral is suggested to evaluate the area, that is,

$$\int_a^b f(t)dt = \frac{b-a}{6} \left(f(a) + 4f\left(\frac{a+b}{2}\right) + f(b) \right) \quad (36)$$

where $f(\theta) = \frac{1}{2}r_p^2(\theta)$ here.

To obtain a simple yet accurate expression of the plastic zone area, Eq (36) is used in $[-\pi, 0]$ and $[0, \pi]$, respectively. Thus we have

$$\begin{aligned} A_P &= \frac{\pi}{6} \left(f(0) + 4f\left(\frac{\pi}{2}\right) + f(\pi) \right) + \frac{\pi}{6} \left(f(-\pi) + 4f\left(-\frac{\pi}{2}\right) + f(0) \right) \\ &= \frac{(1+\kappa)^2}{384c_\Sigma^2 G^2 \pi} \sec^2 \varphi \left[(K_I^2 + K_{II}^2)(K_I^2 + 3K_{II}^2) + (K_I^4 + K_{II}^4) \sin^2 \varphi \right. \\ &\quad \left. + \sin \varphi \left(4K_I K_{II}^2 \sqrt{K_I^2 + K_{II}^2} + 2(K_I^2 + K_{II}^2) \sqrt{(K_I^2 - K_{II}^2)^2} \right) \right] \end{aligned} \quad (37)$$

If $K_I \rightarrow K_{IC}$, then we obtain $A_C = \frac{(1+\kappa)^2}{384c_\Sigma^2 G^2 \pi} \sec^2 \varphi K_{IC}^4 (1 + \sin^2 \varphi + 2 \sin \varphi)$. When $A_P = A_C$, we have a novel fracture criterion. Combining with Eq (35), the initiation angles and fracture loads are obtained, as shown in Figs 10 and 11. It is observed that the initiation angles assessed by the present fracture criterion are greater than those predicted by the MTS fracture criterion, and the fracture loading envelope enlarges with friction angles.

Furthermore, if the radical term in Eq (37) is removed, we have another one simplified fracture criterion, namely MCCA, namely

$$(1 + \sin^2 \varphi) \left(\frac{K_I}{K_{IC}} \right)^4 + 4 \left(\frac{K_I}{K_{IC}} \frac{K_{II}}{K_{IC}} \right)^2 + (3 + \sin^2 \varphi) \left(\frac{K_{II}}{K_{IC}} \right)^4 = (1 + \sin^2 \varphi) \quad (38)$$

It is observed that the original fracture criterion coincides with the simplified one from Fig 11(b), and the predicted fracture loads are consistent with those assessed by the MTS fracture criterion, as illustrated in Fig 12.

It is well known that rock crack surfaces are typically uneven and rough rather than flat and smooth. Xie [50] used fractal geometry to depict the irregularity of the crack surface and merged it with the energy release rate criterion to calculate the critical energy release rate for irregular cracks.

The length of a fractal curve is evaluated by [50]

$$L(\varepsilon_f) = L_0 (\varepsilon_f)^{1-D_f} \quad (39)$$

where L_0 denotes the length of the flat crack, ε_f is the yardstick length, and D_f is the fractal dimension.

By the concept of fractal mechanics mentioned previously, the critical energy release rate is rewritten as

$$G_f = 2 \frac{L(\varepsilon_f)}{L_0} \gamma_s = 2 \gamma_s \left(\frac{1}{\delta_f} \right)^{D_f-1} = G_s \left(\frac{1}{\delta_f} \right)^{D_f-1} \quad (40)$$

where δ_f represents the ratio of similarity. Combining with $G = K^2/E$, it is obtained

$$\begin{cases} K_I^f = K_I \left(\frac{1}{\delta_f} \right)^{(D_f-1)/2} \\ K_{II}^f = K_{II} \left(\frac{1}{\delta_f} \right)^{(D_f-1)/2} \end{cases} \quad (41)$$

Substituting Eq (41) into Eq (38), we obtain the mixed mode fracture criterion of irregular cracks, which is employed to predict the fracture loads in Fig 13. It is also observed from Fig 13(a) that the fracture loads of irregular cracks are less than those of flat cracks, and the crack morphology shall be taken into account to evaluate the stability of cracks.

It is noted that the occurrence environment of rocks has a significant impact on their fracture characteristics. In general, the occurrence environment of rocks may cover many influencing factors. The water rock interaction and thermal-cooling cycles are here taken into account to develop the mixed mode I-II fracture models of rock.

It is noted that rock toughness can deteriorate due to drying-wetting cycles, which need to be considered in the mixed fracture criterion of rock.

Considering K_{IC} related to the number of drying-wetting cycles n , one has

$$\frac{K_{IC}}{K_{IC}^0} = a_1 \ln(n+1) + 1 \quad (42)$$

where K_{IC}^0 represents the initial fracture toughness, and a_1 is the dimensionless parameter that is determined by experiments. Here we obtain $a_1 = -0.2538$ by fitting the experimental data in the literature [21], in terms of Eq (42). It is also found from Fig 14 that the fracture loading envelope decreases with the number increase of drying-wetting cycles.

The environment in which deep rocks are situated is relatively challenging, frequently characterized by heat and cool fluctuations. Accordingly, the investigation for the fracture properties of rocks due to heating and cooling cycles holds considerable importance in the assessment of wellbore stability of geothermal systems. The relation between the fracture toughness and the number of heating and cooling cycles can also be obtained by fitting experimental data [49], using $f(x) = a_1 \exp(-b_1 x) + c_1$.

It is observed from Fig 15 that the fracture load envelope decreases with the number increase of heating and cooling cycles, and the reduction in fracture resistance reduces with the number increase of cycles.

3.2. Rheological fracture criteria by viscoelastic fracture mechanics

In complex environments, rock materials substantially exhibit the rheological characteristics, in which the cracks continue to propagate slowly until they become unstable, resulting in delayed crack instability. The growth of crack in a viscoelastic body consists of three stages: incubation, subcritical crack growth, unstable crack propagation [54], as shown in Fig 16(a). Furthermore, from Fig 16(b), it is found that, if $K_I(0) > K_{IC}$, then the crack instability arises instantly. If $K_I(0) < K_{IC} < K_I(\infty)$, then delayed crack instability will occur at a certain time, and if $K_I(\infty) < K_{IC}$, the crack will not propagate forever. Indeed, elastoplastic fracture mechanics cannot handle the problem of delayed crack instability, whereas viscoelastic fracture mechanics translates viscoelastic problems into elastic problems utilizing the viscoelastic-elastic correspondence principle.

The energy release rate of the viscoelastic body is defined by the corresponding elastic energy release rate multiplied by the time factor of energy release rate,

$$\begin{aligned} G_m^t &= G_m f(t) \\ f(t) &= f_{m\sigma}(t) f_{mu}(t) \end{aligned} \quad (43)$$

where $f(t)$, $f_{m\sigma}(t)$, and $f_{mu}(t)$ denote three time factors of energy release rate, stress intensity factor, and displacement, respectively.

Because of material creep, the displacement of the crack surface gradually increases over time, and thus the stress intensity factor does as well.

Combining with $G_m = K_m^2/E$, we obtain

$$K_m^t = K_m \sqrt{f(t)} = K_m \sqrt{f_{m\sigma}(t) f_{mu}(t)} \quad (44)$$

For the viscoelastic body, the Burgers body model is used to examine the fracture mechanical behaviors of cracks. The time factor of displacement is given by

$$f_{mu}(t) = f_{m\sigma}(t) + C_0 \int_0^t f_{m\sigma}(\tau) d\tau + C_1 \int_0^t f_{m\sigma}(\tau) \lambda \exp(-\lambda \tau) d\tau \quad (45)$$

The Burgers body constitutive model is expressed by

$$\begin{cases} (a_2 D^2 + a_1 D + a_0) S_{ij} = (D^2 + b_1 D) e_{ij} \\ a_0 = \frac{G_2}{2\eta_1 \eta_2}, \quad a_1 = \frac{G_1 \eta_1 + G_2 \eta_1 + G_1 \eta_2}{2\eta_1 \eta_2 G_1} \\ a_2 = \frac{1}{2G_1}, \quad b_1 = \frac{G_2}{\eta_2}, \quad c = 3K_v \end{cases} \quad (46)$$

where D represents the differential operator, K_v denotes the bulk modulus, G_1 , G_2 are the shear modulus, and η_1 , η_2 are the viscosity.

Under constant loading conditions, the time factor of displacement for plane stress problems is read by

$$\begin{cases} f(t) = 1 + C_0 t + C_1 (1 - \exp(-b_1 t)) \\ C_0 = \frac{2a_0 c}{(2a_2 c + 1)b_1}, \quad C_1 = \frac{b_1(2a_1 c + b_1) - 2a_0 c}{b_1^2(2a_2 c + 1)} - 1 \end{cases} \quad (47)$$

Combining with Eq (46), C_0 and C_1 are derived by

$$C_0 = \frac{3G_1 K_v}{(G_1 + 3K_v)\eta_1}, \quad C_1 = \frac{3G_1 K_v}{(G_1 + 3K_v)G_2} \quad (48)$$

Figure 17(c) indicates that the time factor increases with time. Similarly, the standard linear body can be employed, but its time factor gradually approaches a constant.

On the other hand, the configurational stress of viscoelastic body is written by

$$\Sigma_{ij}^t = [1 + C_0 t + C_1(1 - \exp(-b_1 t))] \Sigma_{ij} \quad (49)$$

Substituting Eq (49) into Eq (33), we obtain the crack-tip plastic zone for viscoelastic material. It is observed that the crack-tip plastic zone enlarges with time for mode-I, mode-II, and mixed mode-I/II cracks, in which the parameters used are $G_1 = 30$ GPa, $G_2 = 40$ GPa, $\eta_1 = 300$ GPa · h, $\eta_2 = 500$ GPa · h, $K = 40$ GPa.

Combining with Eq (38), the fracture criterion of viscoelastic body is derived by

$$f^2(t) \left[(1 + \sin^2 \varphi) \left(\frac{K_I}{K_{IC}} \right)^4 + 4 \left(\frac{K_I}{K_{IC}} \frac{K_{II}}{K_{IC}} \right)^2 + (3 + \sin^2 \varphi) \left(\frac{K_{II}}{K_{IC}} \right)^4 \right] = (1 + \sin^2 \varphi) \quad (50)$$

The predicted results are given in Fig 18(d), and it is found that the fracture load envelope decreases with time.

Additionally, if $K_I^t = K_I \sqrt{f(t)}$ and $K_{IC} = (1 - D)K_{IC}^0$, then it is obtained

$$f^2(t) \left[(1 + \sin^2 \varphi) \left(\frac{K_I}{K_{IC}} \right)^4 + 4 \left(\frac{K_I}{K_{IC}} \frac{K_{II}}{K_{IC}} \right)^2 + (3 + \sin^2 \varphi) \left(\frac{K_{II}}{K_{IC}} \right)^4 \right] = (1 - D)^4 (1 + \sin^2 \varphi) \quad (51)$$

It is assumed that the damage variable D is time-dependent, which is defined by [52]

$$D = 1 - \exp(-\alpha t) \quad (52)$$

where α represents the material constant.

Substituting Eq (52) into Eq (51), we can predict fracture loads for damage viscoelastic materials. Figure 19 shows that the fracture loads for damage viscoelastic material is less than those for damage elastic material.

It has been widely observed that water has a specific weakening effects on the mechanical behaviors of rocks [38]. Accordingly, the fracture toughness of rock is related to the chemical corrosion and thermal treatment temperature, and the relation can be determined by experiments. As a typical example, the relation between the fracture toughness and temperature is given by fitting experimental data of rock [56], using $f(x) = a_1 \exp(b_1 x) + c_1 \exp(d_1 x)$, as shown in Fig 20(a) and (b),

$$\frac{K_{IC}}{K_{IC}^0} = 1.36 \exp(-0.0013T) - 0.4809 \exp(-0.0096T) \quad (53)$$

Figure 20 (c) and (d) shows that the fracture load envelope decreases with the temperature increase generally. And if rock is regarded to as a viscoelastic material, its fracture load envelope decreases with time elapse.

Similarly, the relation between the fracture toughness and chemical solution (pH) is also given by fitting experimental data of rock [20], using $f(x, y) = p_{00} + p_{10}x + p_{01}y + p_{20}x^2 + p_{11}xy$, as shown in Fig 21 (a),

$$\frac{K_{IC}^0 - K_{IC}}{K_{IC}^0} = 0.097 - 0.032(\text{pH}) + 0.148t_c + 0.002(\text{pH})^2 - 0.004t_c(\text{pH}) \quad (54)$$

where t_c denotes the corrosion time. It is observed from Fig 21 that the fracture loads increase with pH, but decrease with t_c . Again if considering the viscoelastic behavior of rock, the fracture load envelope decreases with time elapse, as shown in Fig 21(d).

4. Conclusion

Theoretical models have been developed to understand the fracture mechanisms of rock under different environments. The Mohr-Coulomb yield criterion based on configurational stress is deduced, and the plastic zone at the crack tip is assessed. by the plastic zone parameter, a novel mixed fracture criterion is proposed. The effects of drying-wetting cycles, heating-cooling cycles, the thermal effects and chemical corrosion on rock fracture are examined. The conclusions are as follows:

- (1) The physical meaning of configurational stress is the change of total potential energy caused by material element translation.
- (2) The plastic zones at the crack tips of mode I, mode II, and mixed mode I-II are evaluated by using the Mohr-Coulomb yield criteria based on Cauchy stress and configurational stress, respectively. It is found that the configurational stress-based Mohr Coulomb yield criterion in rock predicts better results and the crack-tip plastic zone is continuous at the crack surface and enlarges with the friction angle increase.
- (3) A rock fracture criterion based on the characteristics of the plastic zone at the crack tip is developed. The predicted crack initiation angle and fracture load are all consistent with those assessed by the MTS fracture criterion. The fractal properties of cracks in rock have a substantial impact on the fracture load, and the envelope of fracture load decreases with the number increases of drying-wetting cycles and heating-cooling cycles.
- (4) The fracture load envelope of rock assessed by the present fracture criterion decreases with the thermal treatment temperature increase generally, and the fracture resistance is weaker in acidic environments.

Acknowledgments

Support by the Fundamental Research Funds for the Central Universities (Ph.D. Top Innovative Talents Fund of CUMTB) (No. BBJ2024091) and National Natural Science Foundation of China (Nos. 41172116 and U1261212) is gratefully acknowledged.

CRedit authorship contribution statement

Chao Wang: Conceptualization, Methodology, Software, Writing - original draft. **Hongze Li:** Software, Writing. **J.L. Feng:** Conceptualization, Methodology, Writing - original draft, Writing - review & editing, Supervision, Funding. **Jiaqi Zhang:** Software. **D.J. Li:** Methodology.

Declaration of interests

The authors declare that they have no known competing financial interests or personal relationships that could have appeared to influence the work reported in this paper.

References

- [1] Aliha, M.R.M., Ayatollahi, M.R., 2011. Mixed mode I/II brittle fracture evaluation of marble using scb specimen. *Procedia Engineering* 10, 311–318. doi:10.1016/j.proeng.2011.04.054.
- [2] Anderson, T.L., 2017. *Fracture mechanics: fundamentals and applications*. CRC press, Boca Raton.
- [3] Atkinson, C., Smelser, R.E., Sanchez, J., 1973. Conservation laws and energy-release rates. *Journal of Applied Mechanics* 40, 201–203.
- [4] Atkinson, C., Smelser, R.E., Sanchez, J., 1974. Strain-energy-density factor applied to mixed mode crack problems. *International Journal of fracture* 10, 305–321.
- [5] Bai, Y.L., Wierzbicki, T., 2010. Application of extended Mohr-Coulomb criterion to ductile fracture. *International Journal of Fracture* 161, 1–20. doi:10.1007/s10704-009-9422-8.
- [6] Cannon, S.H., Gartner, J.E., Rupert, M.G., Michael, J.A., Rea, A.H., Parrett, C., 2010. Predicting the probability and volume of postwildfire debris flows in the intermountain western United States. *GSA Bulletin* 122, 127–144. doi:10.1130/B26459.1.
- [7] Chaves, E.W.V., 2013. *Notes on continuum mechanics*. Springer, New York.
- [8] Dascalu, C., Bilbie, G., 2007. A multiscale approach to damage configurational forces. *International Journal of Fracture* 147, 285–294. doi:10.1007/s10704-008-9189-3.
- [9] Erdoga, F., Sih, G.C., 1963. On the crack extension in plates under plane loading and transverse shear. *Journal of Basic Engineering* 85, 519–527. doi:10.1115/1.3656897.

- [10] Eshelby, J.D., 1951. The forces on an elastic singularity. *Philosophical Transactions of the Royal Society of London* 244, 87–112.
- [11] Eshelby, J.D., 1975. The elastic energy-momentum tensor. *Journal of Elasticity* 5, 321–335.
- [12] Gan, Z., Hua, W., Huang, J., Huang, L., Pan, X., Dong, S., 2022. Effect of coupled thermal-chemical on the mixed mode I-II fracture characteristic of sandstone. *Theoretical and Applied Fracture Mechanics* 122, 103619. doi:10.1016/j.tafmec.2022.103619.
- [13] Ghassemi, A., Rawal, A., Zhou, X., 2013. Rock failure and micro-seismicity around hydraulic fracture. *Journal of Petroleum Science and Engineering* 108, 118–127. doi:http://dx.doi.org/10.1016/j.petrol.2013.06.005.
- [14] Gross, D., Kolling, S., Mueller, R., Schmidt, I., 2003. Configurational forces and their application in solid mechanics. *European Journal of Mechanics - A/Solids* 22, 669–692. doi:10.1016/S0997-7538(03)00076-7.
- [15] Guha Roy, D., Singh, T., 2023. Effect of heat-treatment on the pure- and mixed-mode fracture properties of a homogeneous sandstone. *Geomechanics for Energy and the Environment* 33, 100430. URL: <https://www.sciencedirect.com/science/article/pii/S235238082200082X>, doi:https://doi.org/10.1016/j.gete.2022.100430.
- [16] Guo, Q., Su, H., Liu, J., Yin, Q., Jing, H., Yu, L., 2020. An experimental study on the fracture behaviors of marble specimens subjected to high temperature treatment. *Engineering Fracture Mechanics* 225, 106862. doi:10.1016/j.engfracmech.2019.106862.
- [17] Guo, Y., Li, Q., 2017. Material configurational forces applied to mixed mode crack propagation. *Theoretical and Applied Fracture Mechanics* 89, 147–157. doi:10.1016/j.tafmec.2017.02.006.
- [18] Gurtin, M.E., 2002. *Configurational forces as basic concepts of continuum physics*. Springer, New York.
- [19] Gurtin, M.E., Guidugli, P.P., 1996. Configurational forces and the basic laws for crack propagation. *Journal of the Mechanics and Physics of Solids* 44, 905–927. doi:10.1016/0022-5096(96)00014-2.
- [20] Han, T., Shi, J., Chen, Y., Cao, X., 2019. Mechanism damage to mode-I fractured sandstone from chemical solutions and its correlation with strength characteristics. *Pure and Applied Geophysics* 176, 5027–5049. doi:10.1007/s00024-019-02237-w.
- [21] Hua, W., Dong, S., Li, Y., Xu, J., Wang, Q., 2015. The influence of cyclic wetting and drying on the fracture toughness of sandstone. *International Journal of Rock Mechanics and Mining Sciences* 78, 331–335. doi:10.1016/j.ijrmmms.2015.06.010.
- [22] Hussain, M.A., Pu, S.L., Underwood, J.H., 1973. Strain energy release rate for a crack under combined mode I and mode II. *Fracture Analysis, ASTM STP 560, American Society for Testing and Materials*, 2–28.
- [23] Khan, Sma, Khraisheh, M.K., 2004. A new criterion for mixed mode fracture initiation based on the crack tip plastic core region. *International Journal of Plasticity* 20, 55–84. doi:10.1016/S0749-6419(03)00011-1.
- [24] Kienzler, R., Herrmann, G., 1997. On the properties of the eshelby tensor. *Acta Mechanica* 125, 73–91. doi:10.1007/BF01177300.
- [25] Kienzler, R., Herrmann, G., 2002. Fracture criteria based on local properties of the eshelby tensor. *Mechanics Research Communications* 29, 521–527. doi:10.1016/S0093-6413(02)00299-9.
- [26] Kienzler, R.G., Herrmann, G., 2000. *Mechanics in material space with applications to defect and fracture mechanics*. Springer, Berlin Heidelberg New York.
- [27] Liebe, T., Denzer, R., Steinmann, P., 2003. Application of the material force method to isotropic continuum damage. *Computational Mechanics* 30, 171–184. doi:10.1007/s00466-002-0377-0.
- [28] Lim, I.L., Johnston, I.W., Choi, S.K., 1994a. Fracture testing of a soft rock with semi-circular specimens under three-point bending. part 1-mode i. *International Journal of Rock Mechanics and Mining Sciences and Geomechanics Abstracts* 31, 185–197. doi:10.1016/0148-9062(94)90463-4.
- [29] Lim, I.L., Johnston, I.W., Choi, S.K., 1994b. Fracture testing of a soft rock with semi-circular specimens under three-point bending. part 2-mixed-mode. *International Journal of Rock Mechanics and Mining Sciences and Geomechanics Abstracts* 31, 199–212. doi:10.1016/0148-9062(94)90464-2.
- [30] Liu, R., Hou, J., Li, Q., 2020. Material configurational forces applied to mixed-mode fatigue crack propagation and life prediction in elastic-plastic material. *International Journal of Fatigue* 134, 105467.1–105467.11. doi:10.1016/j.ijfatigue.2019.105467.
- [31] Lv, J.N., Li, Q., 2016. Equivalent configurational stress to predict material yielding and crack propagation. *Acta Mechanica* 227, 3055–3065. doi:10.1007/s00707-016-1665-7.
- [32] Maugin, G.A., 1995. Material forces: concepts and applications. *Applied Mechanics Reviews* 48, 213–245. doi:10.1115/1.3005101.
- [33] Maugin, G.A., 2013. Sixty years of configurational mechanics (19502010). *Mechanics Research Communications* 50, 39–49. doi:10.1016/j.mechrescom.2013.03.003.
- [34] Menzel, A., Steinmann, P., 2007. On configurational forces in multiplicative elastoplasticity. *International Journal of Solids and Structures* 44, 4442–4471. doi:10.1016/j.ijsolstr.2006.11.032.
- [35] Mueller, R., Kolling, S., Gross, D., 2002. On configurational forces in the context of the finite element method. *International Journal for Numerical Methods in Engineering* 53, 1557–1574. doi:10.1002/nme.351.
- [36] Noda, H., Dunham, E.M., Rice, J.R., 2009. Earthquake ruptures with thermal weakening and the operation of major faults at low overall stress levels. *Journal of Geophysical Research - Solid Earth* 114, 1–27.
- [37] Paranunzio, R., Chiarle, M., Laio, F., Nigrelli, G., Turconi, L., Luino, F., 2019. New insights in the relation between climate and slope failures at high-elevation sites. *Theoretical and Applied Climatology* 137, 1765–1784. doi:10.1007/s00704-018-2673-4.
- [38] Paterson, M.S., fong Wong, T., 2005. *Experimental Rock Deformation - The Brittle Field*. 2nd edition ed., Springer, Berlin Heidelberg.
- [39] Peng, K., Lv, H., Yan, F., Zou, Q., Song, X., Liu, Z., 2020. Effects of temperature on mechanical properties of granite under different fracture modes. *Engineering Fracture Mechanics* 226, 106838. doi:10.1016/j.engfracmech.2019.106838.
- [40] Rettl, M., Frackl, S., Pletz, M., Tauscher, M., Schuecker, C., 2024. Conforce: Computation of configurational forces for fem results. *SoftwareX* 26, 101718. doi:10.1016/j.softx.2024.101718.
- [41] Rice, J.R., 1979. The mechanics of earthquake rupture, in: Dziewonski, A.M., Boschi, E. (Eds.), *Physics of the Earth's Interior*, Italian Physical Society. Italian Physical Society and North-Holland Publ. Co., pp. 555–649.
- [42] Rice, J.R., Dunham, E.M., Noda, H., 2009. Thermo- and hydro-mechanical processes along faults during rapid slip, in: Hatzor, Y., Sulem, J., Vardoulakis, I. (Eds.), *Meso-Scale Shear Physics in Earthquake and Landslide Mechanics (Proceedings of the Batsheva de Rothschild*

- Seminar on Shear Physics at the Meso-scale in Earthquake and Landslide Mechanics), CRC Press, Ein Gedi, Israel. pp. 3–16.
- [43] Simha, N.K., Fischer, F.D., Shan, G.X., Chen, C.R., Kolednik, O., 2008. J-integral and crack driving force in elasticplastic materials. *Journal of the Mechanics and Physics of Solids* 56, 2876–2895. doi:10.1016/j.jmps.2008.04.003.
 - [44] Steinmann, P., 2002. On spatial and material settings of hyperelastostatic crystal defects. *Journal of the Mechanics and Physics of Solids* 50, 1743–1766. doi:10.1016/S0022-5096(01)00135-1.
 - [45] Theocaris, P.S., Andrianopoulos, N.P., 1982. The mises elastic-plastic boundary as the core region in fracture criteria. *Engineering Fracture Mechanics* 16, 425–432. doi:10.1016/0013-7944(82)90120-5.
 - [46] Wang, C., Feng, J., 2024a. Crack-tip plastic zone and initiation mechanism of rock based on eshelby stress. *Theoretical and Applied Fracture Mechanics* 132, 104477–1–104477–14. doi:10.1016/j.tafmec.2024.104477.
 - [47] Wang, C., Feng, J., 2024b. Fracture criteria and crack initiation mechanism of material based on configurational stress. *International Journal of Applied Mechanics* 16, 2450025. doi:10.1142/S175882512450025X.
 - [48] Wang, C., Feng, J., 2024c. Fracture criteria and rheological fracture mechanism of brittle materials based on eshelby stress. *Acta Mechanica* doi:https://doi.org/10.1007/s00707-024-03979-y.
 - [49] Wu, Q., Xia, Y., Zhao, Y., Wong, L., Wang, S., Feng, G., 2024. An integrated DIC and CPG investigation of the model-I fracture features for granites after cyclic heating-cooling treatments. *Journal of China Coal Society* doi:10.13225/j.cnki.jccs.2023.0974.
 - [50] Xie, H., 1989. The fractal effect of irregularity of crack branching on the fracture toughness of brittle materials. *International Journal of Fracture* 41, 267–274. doi:10.1007/BF00018858.
 - [51] Xue, Y., Ranjith, P., Gao, F., Zhang, Z., Wang, S., 2023. Experimental investigations on effects of gas pressure on mechanical behaviors and failure characteristic of coals. *Journal of Rock Mechanics and Geotechnical Engineering* 15, 412–428. doi:https://doi.org/10.1016/j.jrmge.2022.05.013.
 - [52] Yang, S., Xu, P., Ranjith, P., 2015. Damage model of coal under creep and triaxial compression. *International Journal of Rock Mechanics and Mining Science* 80, 337–345. doi:10.1016/j.ijrmms.2015.10.006.
 - [53] Yang, S.Q., Jing, H.W., 2011. Strength failure and crack coalescence behavior of brittle sandstone samples containing a single fissure under uniaxial compression. *International Journal of fracture* 168, 227–250. doi:10.1007/s10704-010-9576-4.
 - [54] Zhang, C.Y., 2006. Viscoelastic fracture mechanics. Science Press, Beijing.
 - [55] Zhao, Y., Wang, Y., Wang, W., Tang, L., Liu, Q., Cheng, G., 2019. Modeling of rheological fracture behavior of rock cracks subjected to hydraulic pressure and far field stresses. *Theoretical and Applied Fracture Mechanics* 101, 59–66. doi:10.1016/j.tafmec.2019.01.026.
 - [56] Zuo, J., Xie, H., Dai, F., Ju, Y., 2014. Three-point bending test investigation of the fracture behavior of siltstone after thermal treatment. *International Journal of Rock Mechanics and Mining Sciences* 70, 1365–1609. doi:10.1016/j.ijrmms.2014.04.005.

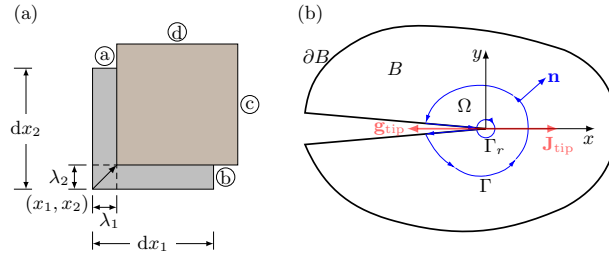


Figure 1: Illustration for infinitesimal element translation and the crack-tip configurational force

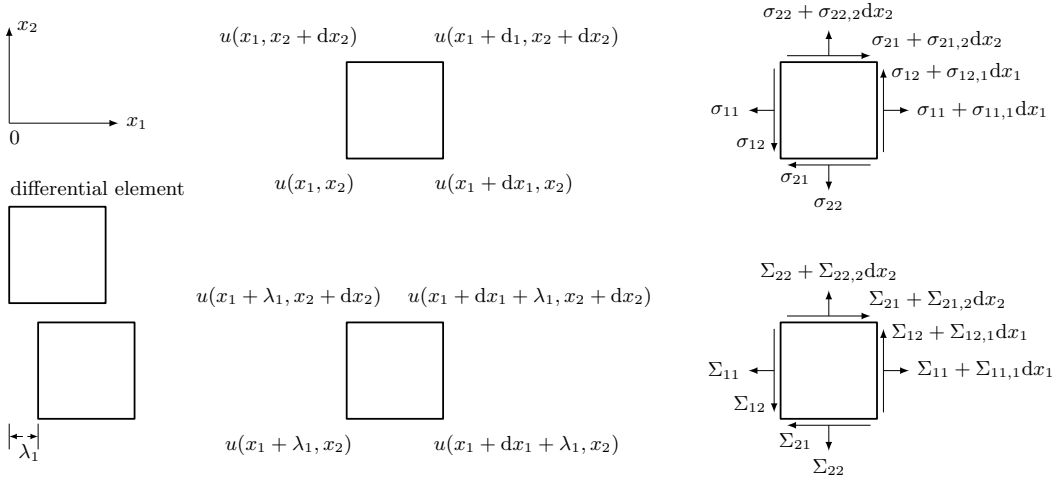


Figure 2: Element node displacement and stress components

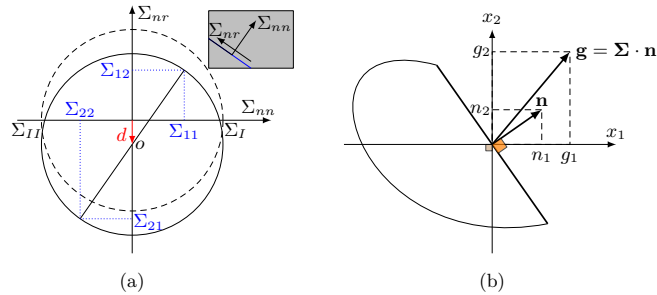


Figure 3: Mohr's circle of configurational stress

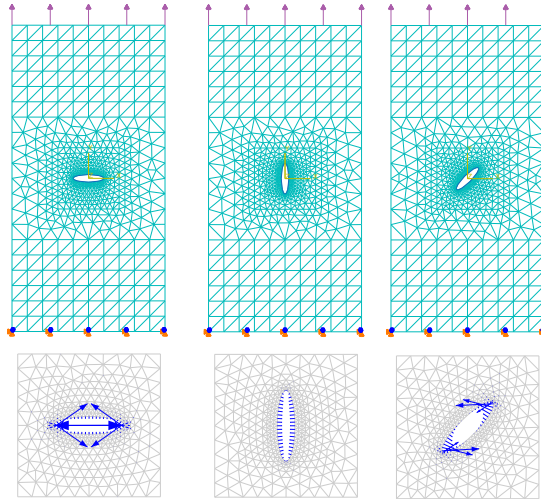


Figure 4: Illustration for the vectors of nodal configurational forces

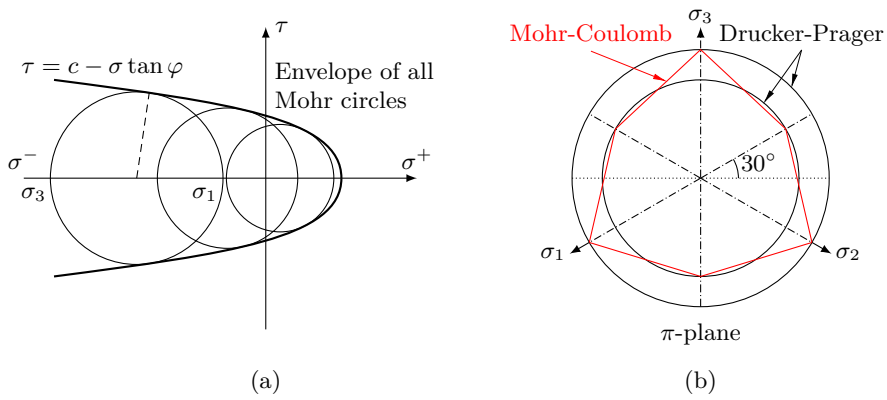


Figure 5: Illustration for Mohr-Coulomb yield surface

Hydraulic Crack Initiation

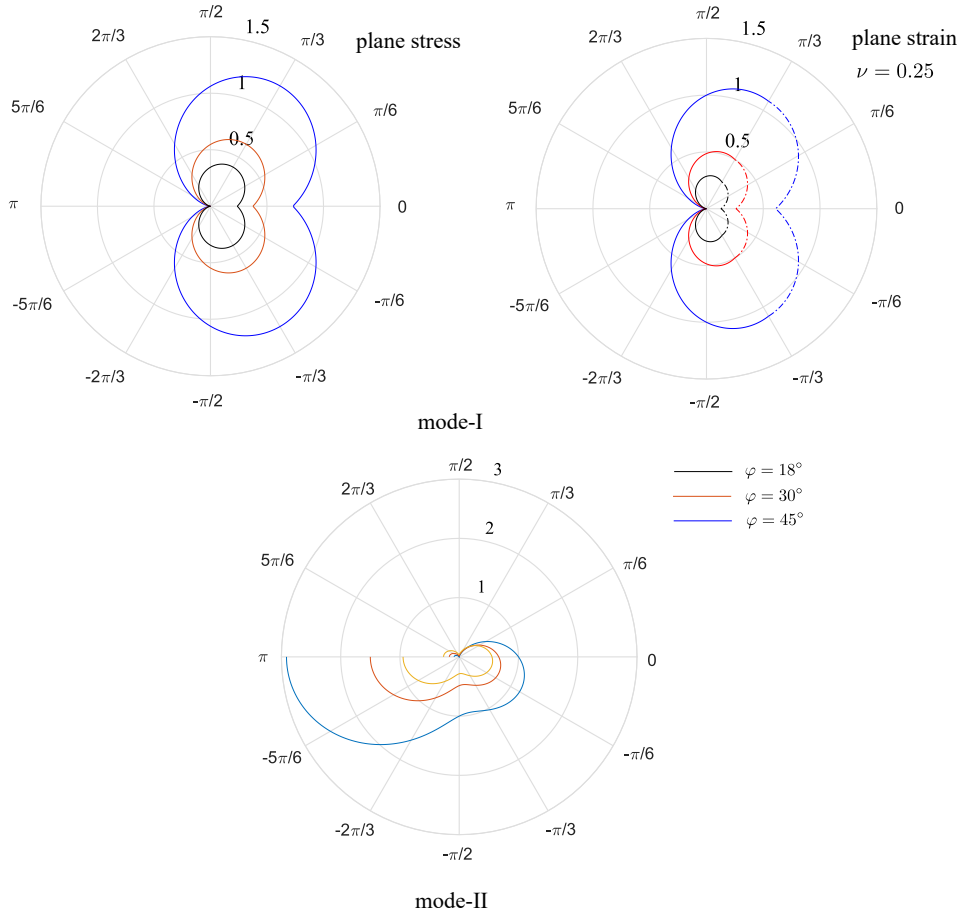


Figure 6: The mode-I and II crack-tip plastic zones assessed by the Mohr-Coulomb yield criterion

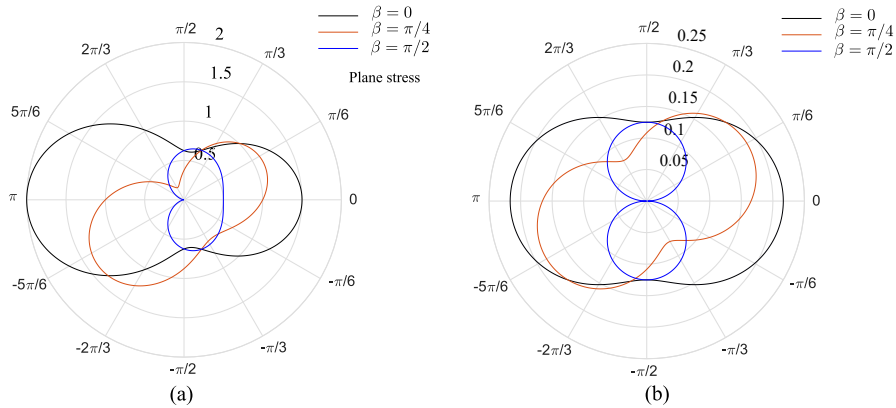
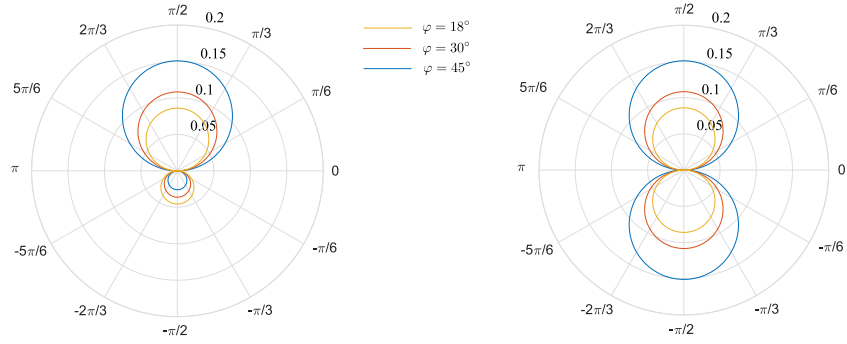
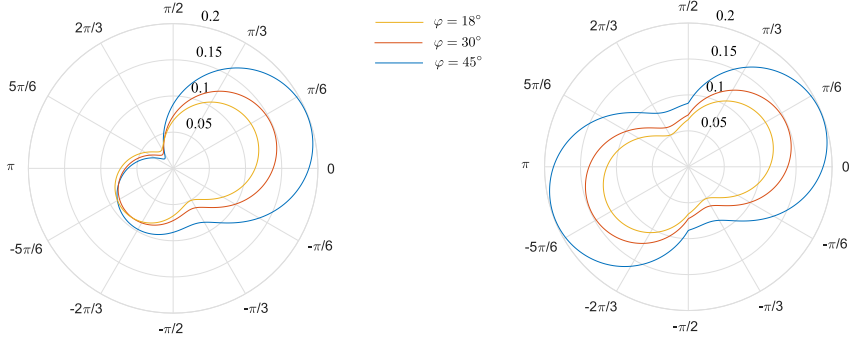


Figure 7: The crack-tip plastic zone assessed by (a) Mises stress and (b) Mises configurational stress

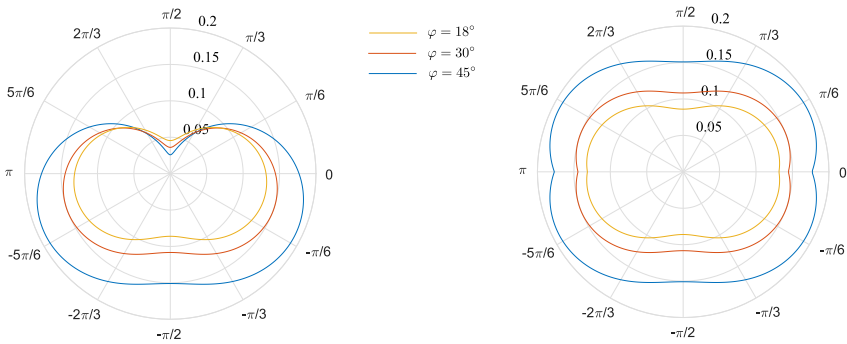
Hydraulic Crack Initiation



(a) $\beta = 0$



(b) $\beta = \frac{\pi}{4}$



(c) $\beta = \frac{\pi}{2}$

Figure 8: Crack-tip plastic zones assessed by the Mohr-Coulomb yield criterion based on configurational stress

Hydraulic Crack Initiation

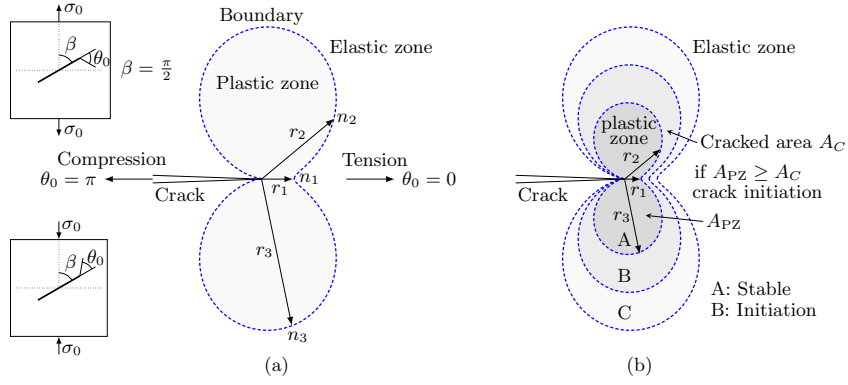


Figure 9: The present fracture criterion based on the crack-tip plastic zone

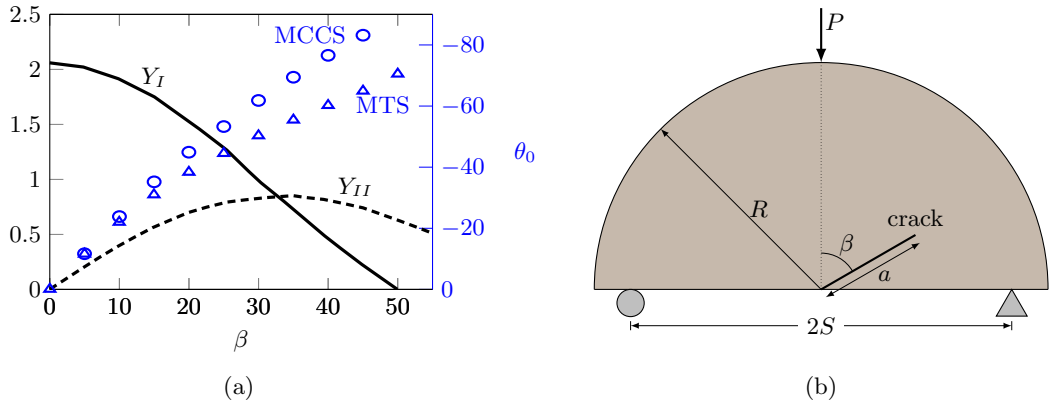


Figure 10: The initiation angles predicted by the present fracture criterion

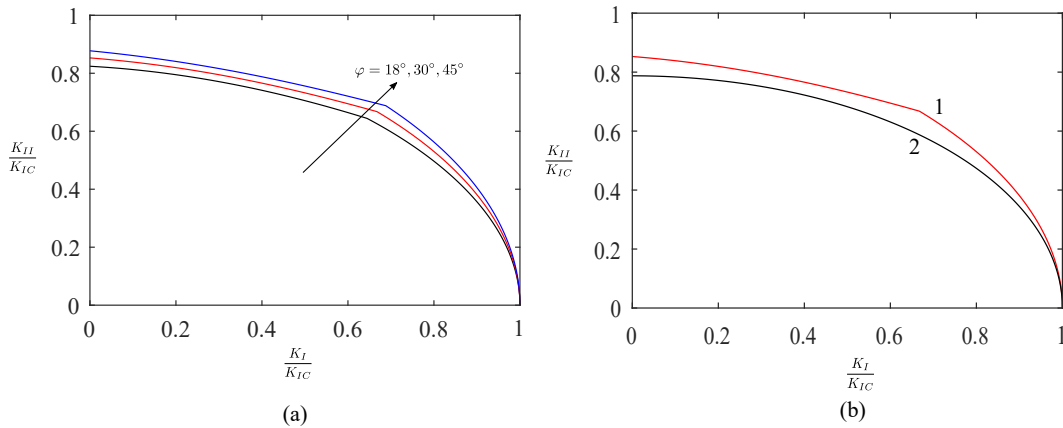


Figure 11: Fracture loads assessed by the present fracture criterion (1,2 represent the original fracture criterion and the simplified one)

Hydraulic Crack Initiation

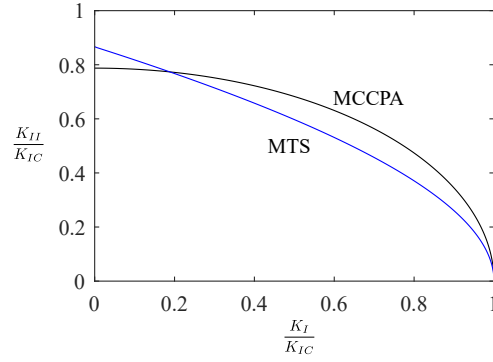


Figure 12: Fracture loads determined by the MTS and present MCCPA fracture criteria

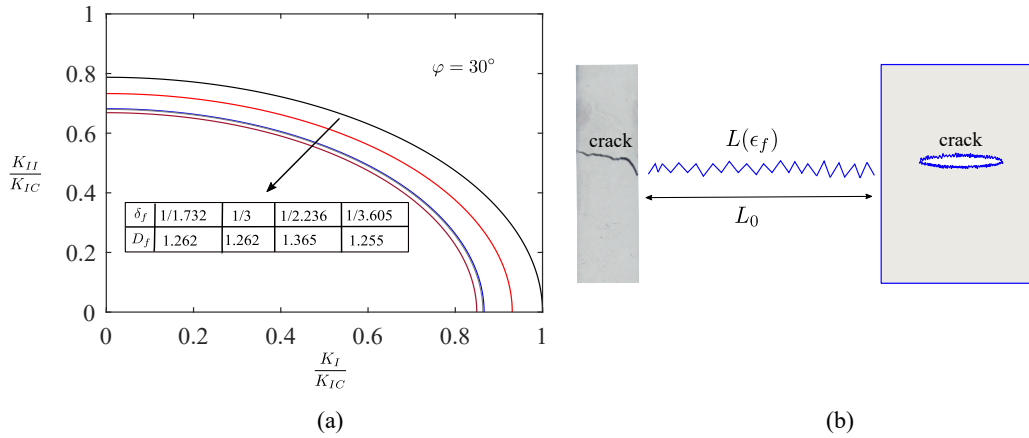


Figure 13: Fracture loads for fractal cracks assessed by the present fracture criterion

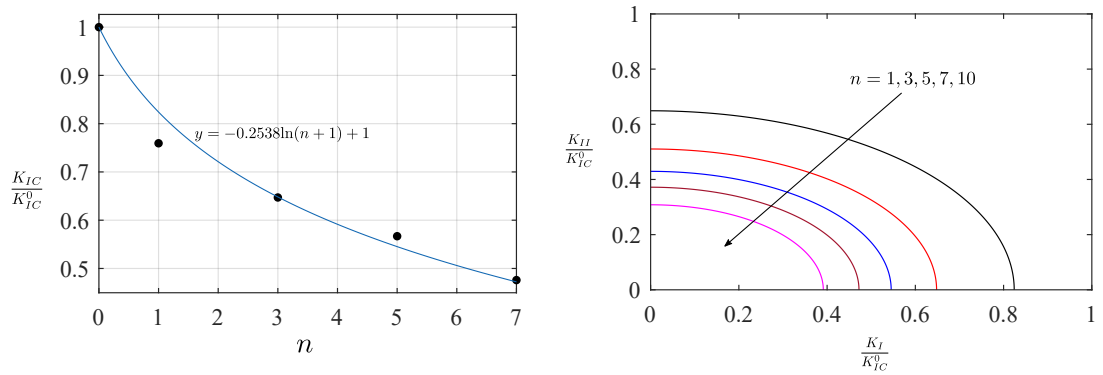


Figure 14: Fracture loads of rock under drying and wetting assessed by the present fracture criterion

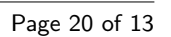


Figure 16: Illustration for material rheological fracture

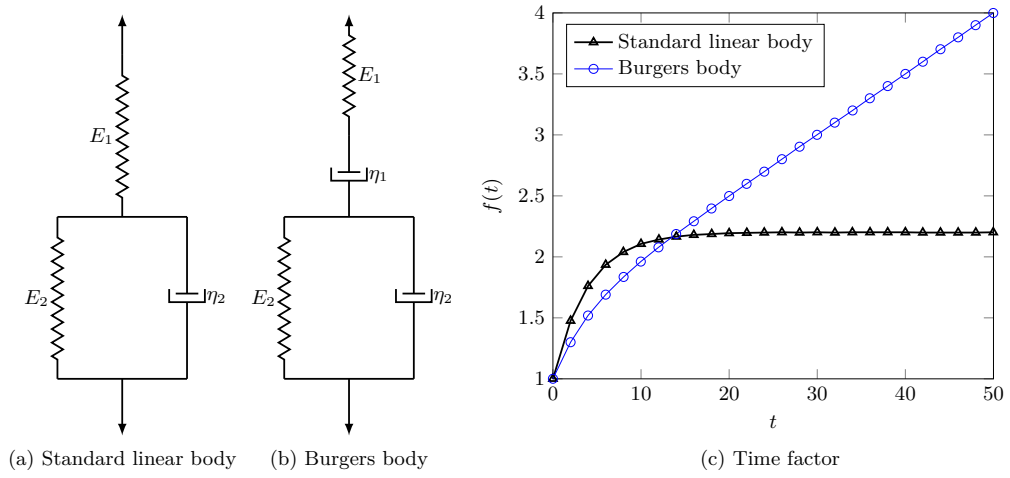


Figure 17: The rheological models for standard linear body and Burgers body

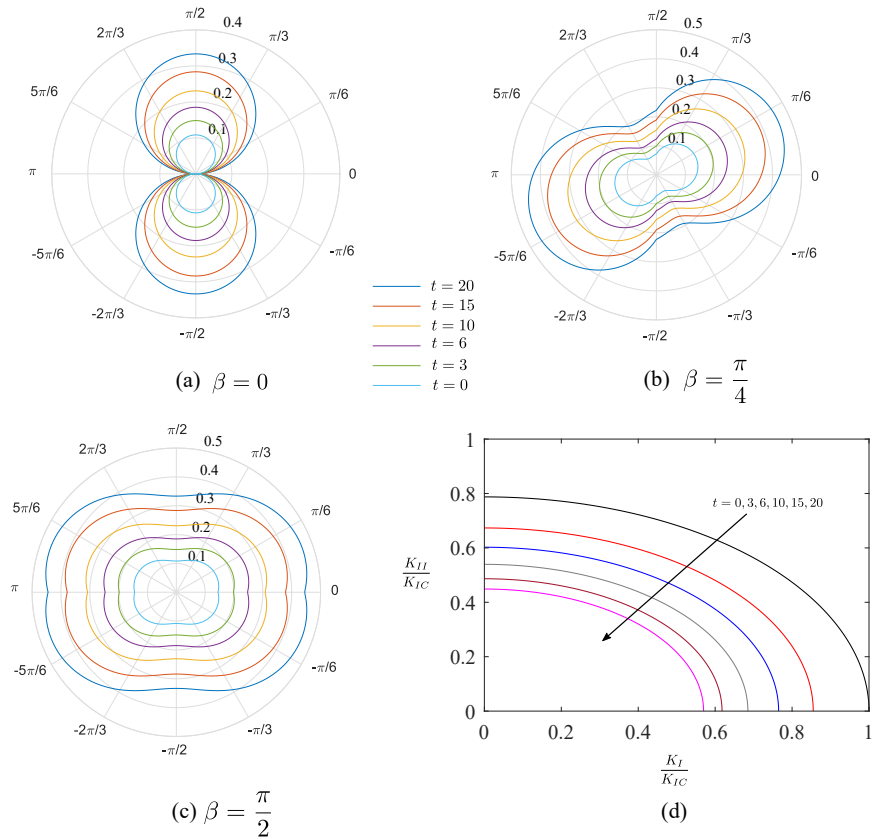


Figure 18: The crack-tip plastic zone and fracture loads at different times (time: h)

Hydraulic Crack Initiation

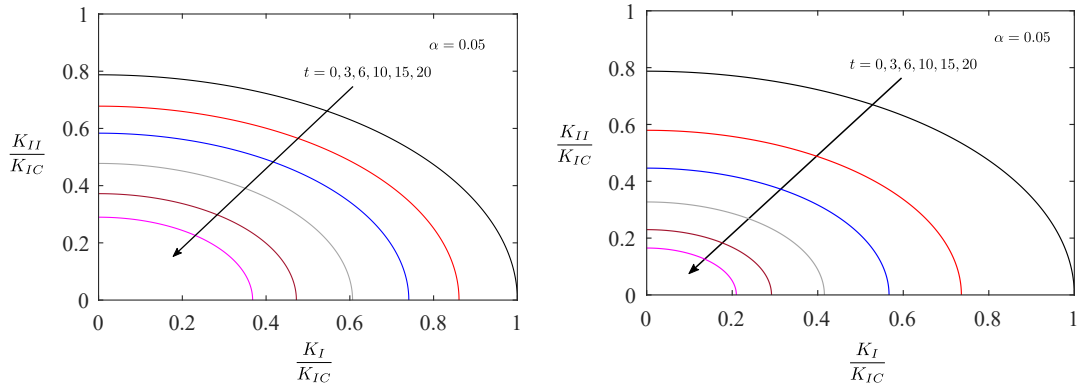


Figure 19: Fracture loads of damaged rock predicted by the present fracture criterion: (a) only considered toughness degradation, and (b) considered both toughness degradation and viscoelastic behavior (time: h)

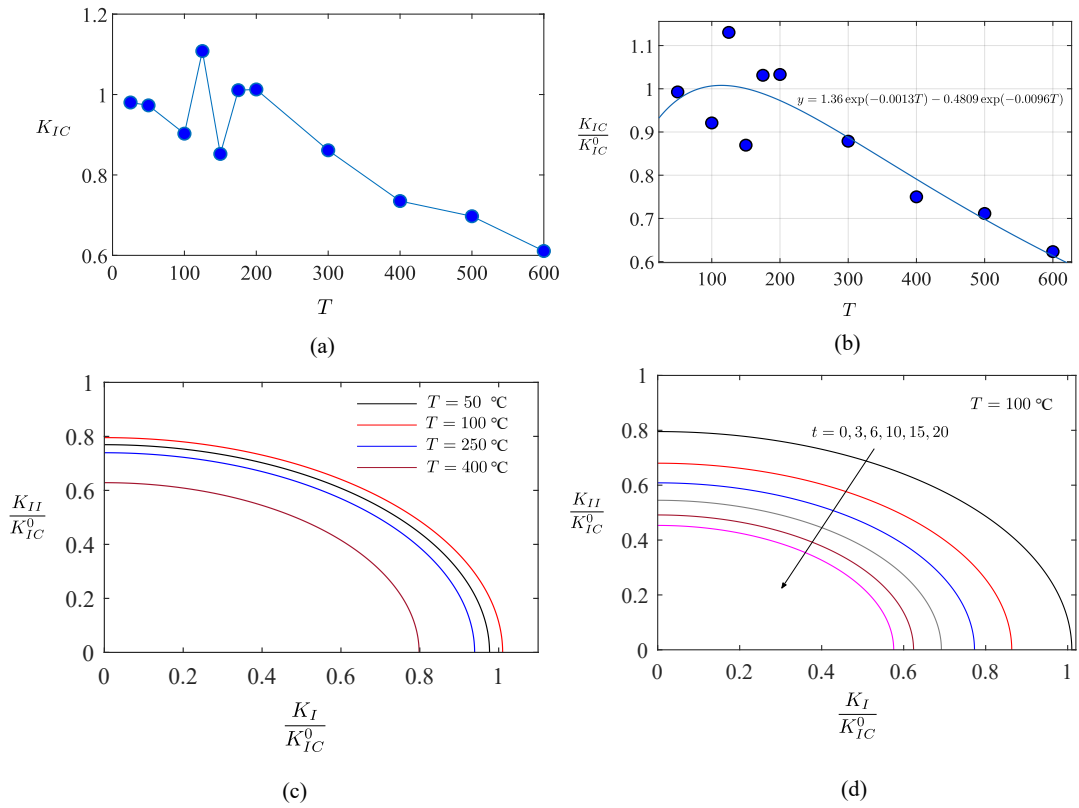


Figure 20: Fracture loads of thermal treated rock predicted by the present fracture criterion (time: h)

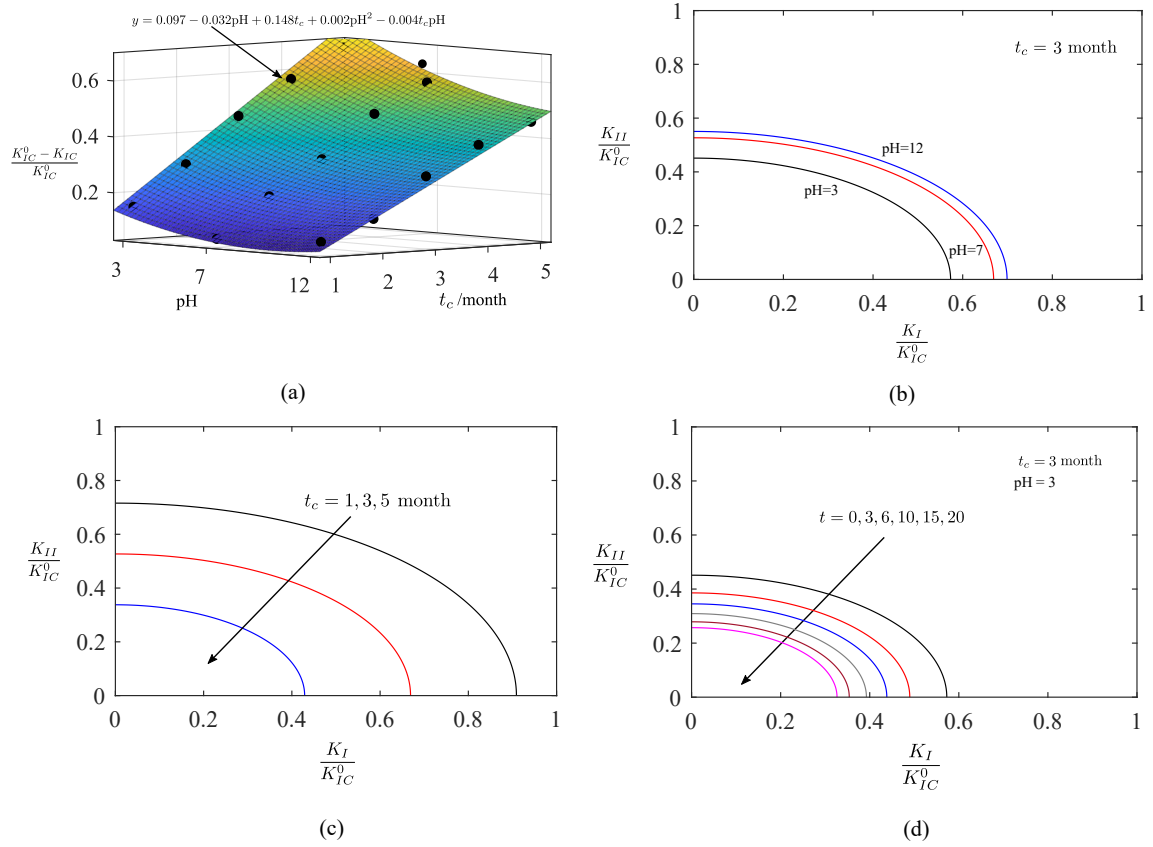


Figure 21: Fracture loads of chemically treated rock assessed by the present fracture criterion (time: h)